Taylor & Francis
Taylor & Francis Group

TECHNICAL PAPER

OPEN ACCESS | Check for updates

Incorporating meander to account for the impact of low winds in area source modeling; AERMOD as a case study

Akula Venkatram[a], Gavendra Pandey[b], and Saravanan Arunachalam[b]

[a]Department of Mechanical Engineering, University of California, Riverside, CA, USA; [b]Institute for the Environment, The University of North Carolina at Chapel Hill, Chapel Hill, NC, USA

ABSTRACT
A variety of sources of pollutant emissions can be represented as area sources. These include manure lagoons, landfills, wastewater treatment ponds, and highways. A group of point sources can also be treated as an area source. The impact of an area source is usually computed by representing the area source as a set of line sources perpendicular to the wind direction. As for point sources, the Gaussian horizontal concentration distribution used to compute the contributions of the line sources is likely to overestimate ground-level concentrations when the wind speed is comparable to the standard deviation of the horizontal velocity fluctuations. A variety of methods are used to mitigate this overestimation under these conditions, referred to as meander. As an example of one these approaches, we examine that of AERMOD, EPA's regulatory model. AERMOD includes meander in modeling the impact of point and volume sources, but has not yet incorporated it into AERMOD's area source algorithm. This paper describes an approach to include meander in AERMOD's area source algorithm and demonstrates its impact on concentrations associated with area sources.

Implications: Inclusion of wind direction meander in modeling dispersion when the wind speed is low is important in ensuring that AERMOD does not overestimate concentrations under these conditions. In view of the importance of area sources of pollution, the results presented in this paper represent a potential enhancement of AERMOD's ability to estimate the upper end of the concentration distribution, which forms the basis of the regulatory acceptance of the model.

Introduction

When the mean wind speed is comparable to the standard deviation of the horizontal velocity fluctuations, the wind direction is uncertain and the concentration distribution in the horizontal might not be Gaussian. In addition, the friction velocity estimated with Monin-Obukhov (M-O) similarity underestimates the measured value. Consequently, the concentration is likely to be overestimated when the wind speed is low.

Several approaches have been used to model dispersion under low winds. For example, Lagrangian particle models have been used to simulate dispersion under low wind speed conditions by Brusasca, Tinarelli, and Anfossi ([1992](#)), Oettl, Almbauer, and Sturm ([2001](#)) and Anfossi et al. ([2006](#)). The trajectories of these particles are governed by measured wind speed and turbulence levels as a function of time. Another approach (Cirillo and Poli [1992](#); Sharan and Yadav [1998](#)) is based on modifying the three-dimensional diffusion equation to include along-wind diffusion, which becomes important for low wind speeds.

In this paper, we focus on an approach that has been adopted by two of the most commonly used regulatory dispersion models, AERMOD (AMS/EPA Regulatory Model, Cimorelli et al. [2005](#)) and ADMS (Atmospheric Dispersion Modeling System, Carruthers et al. [1994](#)). This paper examines AERMOD's approach, referred to as "meander", which is included in computing dispersion from point and volume sources. However, meander is not considered in estimating concentrations from area sources. This paper proposes a method to include meander in AERMOD's area source algorithm.

AERMOD reduces overestimation of concentrations at low wind speeds by 1) modifying the calculation of the friction velocity using an approach suggested by Qian and Venkatram ([2011](#)) to ensure that the friction velocity does not approach zero when the mean wind speed is close to zero, 2) using a minimum value of the standard deviation of the horizontal velocity fluctuations, $\sigma_v = 0.3\ m/s$, and 3) incorporating a meander algorithm (Cimorelli et al. [2005](#)) that combines two horizontal

concentration distributions: a Gaussian distribution corresponding to a plume, and a uniform distribution over all directions or 360^0 as shown in Figure 1. Hanna and Chowdhury (2014) show that these modifications reduce the overestimation of maximum concentrations measured in two field studies designed to study dispersion at wind speeds close to 1 m/s at a height of 10 m.

The concentration associated with the plume is given by the commonly used Gaussian formulation:

$$C_p(x_r, y_r, z_r) = \frac{Q}{2\pi U_s \sigma_z \sigma_y} \exp\left(-\frac{(y_r - y_s)^2}{2\sigma_y^2}\right)$$
$$\left[\exp\left(-\frac{(z_r - z_s)^2}{2\sigma_z^2}\right) + \exp\left(-\frac{(z_r + z_s)^2}{2\sigma_z^2}\right)\right]$$
$$(1)$$

where Q is the emission rate, U_s is the mean scalar wind speed evaluated at mean plume height (See Cimorelli et al. 2005 for details), σ_y and σ_z are the horizontal and vertical plume spreads, and the subscripts "s" and "r" refer to source and receptor. The vertical and horizontal plume spreads depend on the downwind distance $x_r - x_s$, and micrometeorological variables (Cimorelli et al. 2005).

The uniform distribution, C_r, is given by the expression

$$C_r(x_r, y_r, z_r) = \frac{Q}{2\pi r} \frac{V(z_s, z_r, r)}{U_s}$$
$$V(z_s, z_r, r) = \frac{1}{\sqrt{2\pi}\sigma_z(r)} \left(\exp\left(\frac{(z_r - z_s)^2}{2\sigma_z^2}\right)\right.$$
$$\left. + \exp\left(\frac{(z_r + z_s)^2}{2\sigma_z^2}\right)\right)$$
$$(2)$$
$$r = \left(x^2 + y^2\right)^{1/2},$$

where r is the distance from the source to the receptor. These two distributions are weighted according to the magnitude of the standard deviation of horizontal velocity fluctuations, σ_v, relative to the mean vector wind speed

$$C(x_r, y_r, z_r) = f_r C_r(x_r, y_r, z_r) + (1 - f_r) C_r(x_r, y_r, z_r)$$
where
$$f_r = \frac{2\sigma_v^2}{U_s^2} \text{ and } U_s^2 = U_v^2 + 2\sigma_v^2$$
$$(3)$$

Note that Equation (3) provides the relationship between the vector mean wind speed, U_v, and the mean scalar wind speed, U_s assuming that $\sigma_u = \sigma_v$. We see that the maximum value of the weighting factor f_r is unity when the wind speed distribution is uniform across 0 to 2π when the vector mean wind speed, U_v, is zero.

A variety of sources of pollutant emissions can be modeled as area sources. These include manure lagoons, landfills, wastewater treatment ponds, and highways. A group of point sources can also be treated as an area source. This paper describes an approach to include meander in the area source model in AERMOD, and demonstrates its impact on ground-level concentrations. We begin with a brief description of the area source calculation in AERMOD.

Treatment of area sources

AERMOD estimates concentrations associated with an area source by representing it with a convex polygon. The calculations are performed using a co-ordinate system in which the x-axis is along the near-surface wind vector. The contribution of the area source to the concentration at a receptor at (x_r, y_r, z_r) is computed by representing the area by a set of equally spaced line sources that span the along-wind width of the area source. Figure 2 depicts one of these line sources.

The concentration caused by a single line can be written as

$$C(x_r, y_r, z_r) = q F_z(x_r - x_l, z_s, z_r)(erf(t_2) - erf(t_1))/2$$
where
$$t_1 = \frac{y_r - y_b}{\sqrt{2}\sigma_y(x_r - x_l)}, \text{ and } t_2 = \frac{y_r - y_e}{\sqrt{2}\sigma_y(x_r - x_l)}$$
$$(4)$$

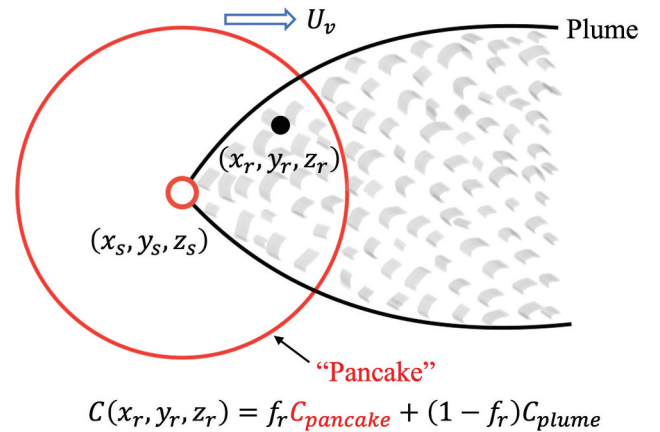$$C(x_r, y_r, z_r) = f_r C_{pancake} + (1 - f_r) C_{plume}$$

Figure 1. The concentration at a receptor (x_r, y_r, z_r) consists of contribution from a plume aligned in the direction of the mean wind vector and a 'pancake' plume. The weighting factor depends on the magnitude of the standard deviation of horizontal velocity fluctuations relative to the magnitude of the wind vector.
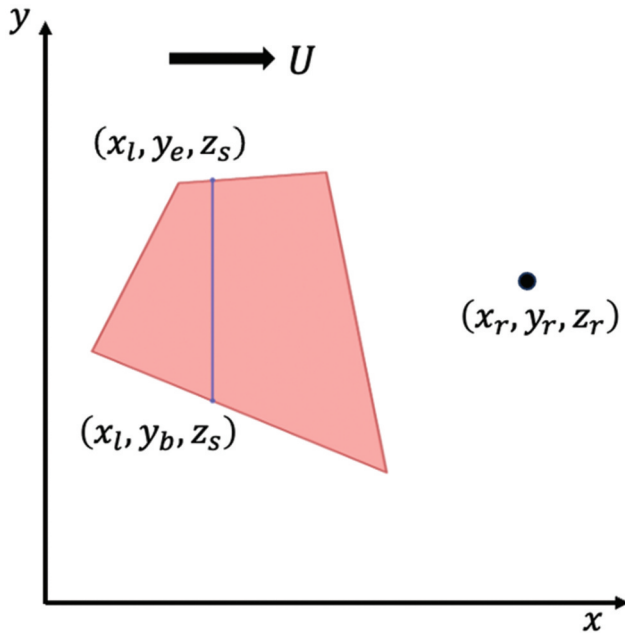
Figure 2. Area source representation. The red polygon is the area source. The blue line is a line source that is perpendicular to the surface wind. The black arrow represents the near-surface wind direction.

Figure 3. Contribution of an element of the line source to the receptor (x_r, y_r, z_r) using the meander formula.

The vertical distribution of the concentration, F_z, which does not vary along y, is commonly described with a Gaussian distribution in AERMOD.

The contribution of a set of N line sources on an area source to the concentration at a receptor is written as

$$C(x_r, y_r, z_r) = q \sum_{i=1}^{i=N} F_z(x_r - x_l^i, z_s, z_r) F_y(x_r - x_l^i) \quad (5)$$

where x_l^i is the x-co-ordinate of the ith line source with a length l^i. The sum in Equation (5) is conducted in steps in which the number of line sources is inserted between the existing set of lines. The value of the sum in each step is combined with that calculated in the previous step by weighting each of them by the corresponding total length of the line sources.

The convergence of the sum can be speeded up by treating the sum as an integral expressed numerically using the trapezoidal rule (Press et al. 1996). After a specified number of successive integrals are computed, they are used to compute the value of the integral at zero spacing between lines using fifth-order polynomial extrapolation based on Neville's algorithm (Press et al. 1996). If the relative interpolation error is greater than 10^{-5}, another integral is computed by updating the previous value of the integral. This value is then used with the previous four values to estimate the value at zero spacing and the corresponding relative error. Details of the numeri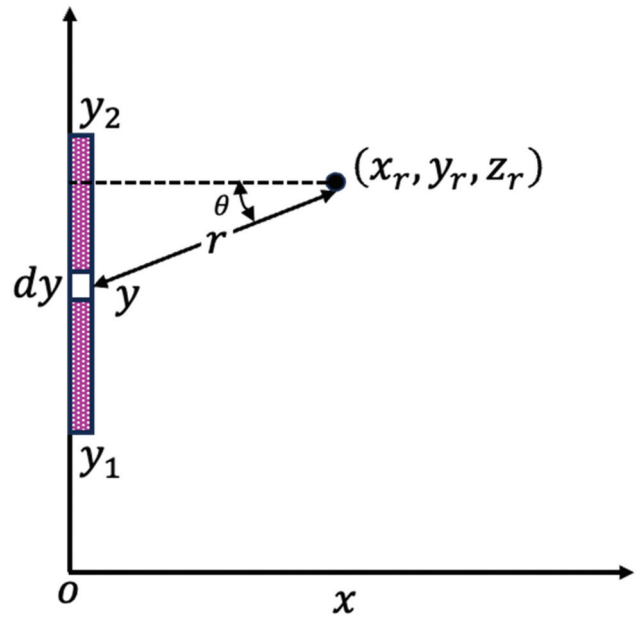cal procedure are described by Venkatram and Thiruvenkatachari (2023). The inclusion of meander in the line source algorithm is described next.

Including meander

Figure 3 shows a line source and the impact of the element dy on the concentration at the receptor (x_r, y_r, z_r). We assume that the line source is at a height z_s, and the receptor at z_r.

Then the concentration at the receptor caused is given by

$$C(x_r, y_r, z_r) = \int_{y_1}^{y_2} \frac{q\,dy}{2\pi r} \frac{V(z_s, z_r, r)}{U_s}, \quad (6)$$

where q is the emission rate per unit length of the line source. Note that the integrand in Equation (6) is Equation (2), the concentration associated with an elemental point source of strength $Q = qdy$ at a distance r from the receptor. The integral expresses the sum of the contributions of the elemental point sources that make up the line source.

Note that the vertical spread, σ_z, is a function of the radial distance from the source to receptor, $r = (x^2 + y^2)^{\frac{1}{2}}$, as well as micrometeorology. This integral cannot be evaluated analytically for arbitrary σ_z. Evaluating the integral numerically will add computing time to the already resource-demanding area source algorithm. Thus, it is useful to examine the utility of an

analytical approximation derived by first assuming that both and receptor are at ground level, $z_s = z_r = 0$,

$$C(x_r, y_r, z_r) = \int_{y_1}^{y_2} \frac{qdy}{2\pi r} \sqrt{\frac{2}{\pi}} \frac{1}{\sigma_z(r)U_s}. \quad (7)$$

Equation (7) can be integrated analytically by assuming that the vertical spread grows linearly with r, $\sigma_z = \sigma_w r/U_s$, which allows us to write Equation (7) as

$$C(x_r, y_r, z_r) = \int_{y_1}^{y_2} \frac{qdy}{2\pi r^2} \sqrt{\frac{2}{\pi}} \frac{1}{\sigma_w}. \quad (8)$$

Using the angle θ shown in Figure 3, we substitute $y = x_r \tan(\theta)$ and $r = x_r/\cos(\theta)$ into Equation (8) to obtain

$$C(x_r, y_r, z_r) = \int_{\theta_1}^{\theta_2} \frac{qd\theta}{2\pi\sigma_w x_r} \sqrt{\frac{2}{\pi}} = \sqrt{\frac{2}{\pi}} \frac{q(\theta_2 - \theta_1)}{2\pi\sigma_w x_r}. \quad (9)$$

Using $\sigma_z(x_r) = \sigma_w x_r/U_s$, Equation (9) can be written as

$$C(x_r, y_r, z_r) = \sqrt{\frac{2}{\pi}} \frac{q}{\sigma_z(x_r)U_s} \left(\frac{\theta_2 - \theta_1}{2\pi} \right)$$
$$\theta_2 - \theta_1 = \tan^{-1}\left(\frac{y_2 - y_r}{x_r} \right) - \tan^{-1}\left(\frac{y_1 - y_r}{x_r} \right) \quad (10)$$

Notice that $(\theta_2 - \theta_1)$ is simply the angle subtended by the line at the receptor. For an infinitely long line, the subtended angle is π, and the concentration at the receptor, (x_r, y_r), is 1/2 the value one would obtain if the wind was blowing perpendicular to the line. So, we propose the following approximation to the integral in Equation (6),

$$C(x_r, y_r, z_r) = \frac{qV(x_r, z_r, z_s)}{U_s} \left(\frac{\theta_2 - \theta_1}{2\pi} \right). \quad (11)$$

The vertical distribution function, V, is evaluated at x_r, the perpendicular distance of the receptor to the line.

The next section examines the impact of including meander in the area source algorithm and the errors associated with the approximations to the numerical integral.

Impact of meander

The meteorological inputs used in the simulations are computed by specifying the variables, $U_s, L,$ and z_0, at $z_{ref} = 10$ m. These variables are used compute the surface

friction velocity, u_*, the standard deviation of the horizontal velocity fluctuations, σ_v, which are in turn are used to compute the vertical and horizontal spreads of the plume (Cimorelli et al. 2005). In the simulations that follow, we take $z_0 = 0.01$ $m, z_s = z_r = 1$ m, and $\theta = 225^0$, and the other parameters are allowed to vary. As in AERMET (AERMOD's meteorological processor), the minimum $\sigma_v = 0.3$ m/s. The stability of the surface boundary layer is characterized with the M-O length, $L = -\frac{T_0}{g} u_*^3/kQ_0$, where T_0 is the 10 m temperature, g is the acceleration due to gravity, $k = 0.4$ is the von-Karman constant, u_* is the surface friction velocity, and Q_0 is the surface kinematic heat flux. The absolute magnitude of the M-O length, $|L|$, is roughly the height above ground that is dominated by shear production of turbulence. So, a large L signifies a deep "neutral" surface layer. A negative L corresponds to an "unstable" surface layer in which the height above $|L|$ is dominated by buoyancy production of turbulence. A "stable" surface layer is described by a positive L is one in which shear production is dominant below L, while the negative heat flux suppresses turbulence above L.

The reference case is the simulation that does not include meander. The meteorological conditions and relevant statistics for the simulations discussed here are listed in Table 1. The impact of meander is quantified in terms of three statistics: the mean of the concentration without meander, the fractional bias and the standard deviation of the differences between the cases without and with meander.

Figure 4 shows the impact of meandering on plume concentrations under near neutral conditions when L = −1000 m. The scalar wind speed is taken to be $U_s = 0.5$ m/s to allow the contribution of meander to the concentrations, 72%, to dominate the plume contribution. Note that the contribution of meander to the concentration at 0.72 does not vary with stability because its value is determined by the minimum value of $\sigma_v = 0.3$ m/s, which is larger than the value of σ_v computed from M-O similarity.

Panels a and b show that, as expected, the major effect of meander is upwind of the source. Panel c shows that concentrations that are small compared to the mean value are enhanced with meandering, while concentrations that are much larger than the mean value are decreased relative to the reference plume case. Table 1 indicates that meandering gives rise to a fractional bias of

Table 1. Meteorological inputs and differences associated with including meander in the area source algorithm. f_r is the meander weighting factor defined in equation 3.

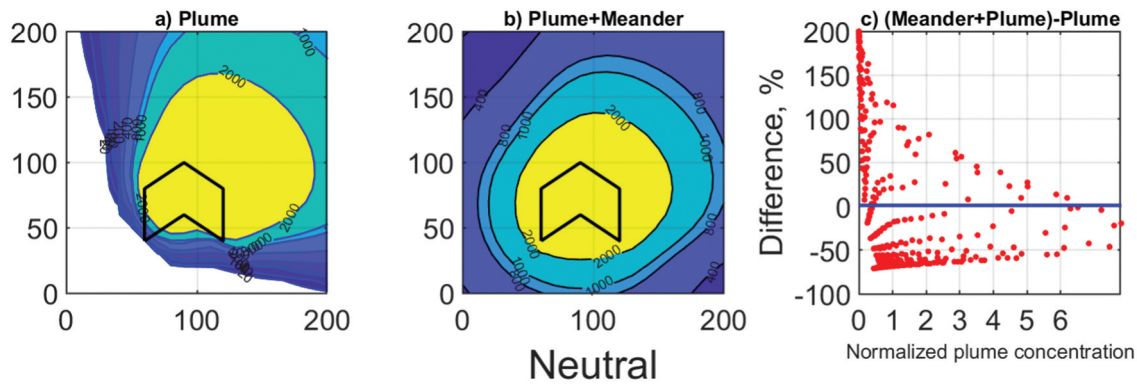| Simulation Number	Scalar Wind Speed m/s	M-O length (m)	f_r	Plume Mean $\mu g/m^3$	Fractional Bias %	Standard Deviation of Difference/Mean
1	0.5	−1000	0.72	1905	−8.2	0.82
2	0.5	−10	0.72	1280	−2.6	0.83
3	0.5	10	0.72	3001	−16.8	0.85

Figure 4. Concentration pattern associated with the polygon area source under neutral conditions. The distances shown in the figure are expressed in meters. The emission rate from the source is 1 g/s, and the units of concentration are $\mu g/m^3$. The wind speed = 0.5 m/s, M-O length= −1000 m correspond to simulation 1 of Table 1. In panel c, the plume concentration is normalized with the mean of the plume spatial field.

−8.2%; meander reduces the concentrations. The standard deviation of the differences is 0.82 of the mean.

In simulation 2, the M-O length is −10 m, signifying unstable conditions. Figure 5 shows that the modification of the spatial pattern by meandering is similar to that of the neutral case. The FB is −2.6% and the standard deviation is 0.83 of the mean without meander. In simulation 3, illustrated in Figure 6, L = 10 m corresponds to stable conditions. The FB is now −16.8%, and the standard deviation is 0.85. The simulations considered here show that meander has its largest impact during stable conditions, and its least during unstable conditions.

As indicated earlier, the introduction of meandering increases the computing demand of the already resource-hungry area source algorithm. In the simulations considered here, the ratio of computing times with to without meander ranged from a factor of 30 for the stable case, to a factor of 40 for the unstable case. While these statistics will vary with the specifics of the processor, it is clear that

the approximation of Equation (11) will reduce computing time significantly if it is found to yield results that are close to that obtained by the numerical integration of Equation (6). The next section compares the results from the numerical and approximate analytical formulations for meander.

Approximating meander

Figure 7 compares the results from the approximation, Equation (11), with the exact solution corresponding to the numerical integration of Equation (6) under conditions when the approximation is valid: $z_r = z_s = 0$, and the stability is neutral so that σ_z. The small differences between the two results, shown in panel c, which occur at concentrations close to zero, are related to the errors in the numerical integration.

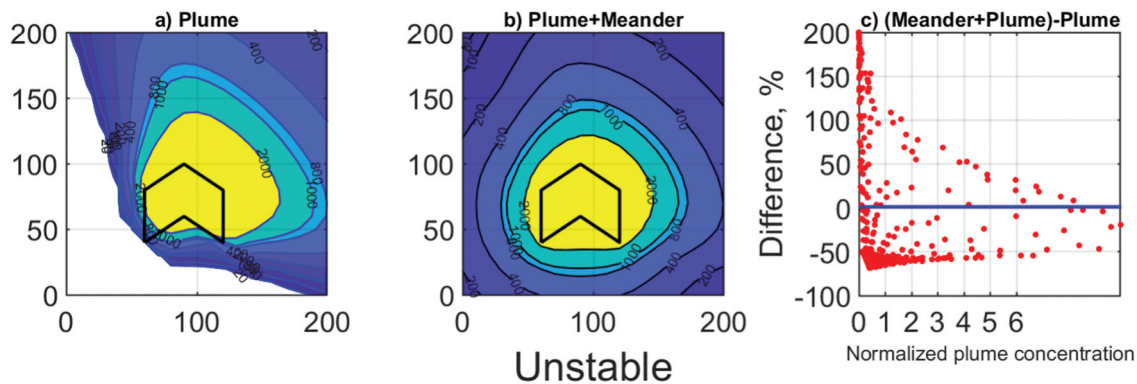Figure 8 shows that the differences between the exact and approximate cannot be neglected when the source

Figure 5. Concentration pattern associated with the polygon area source under unstable conditions. The distances shown in the figure are expressed in meters. The emission rate from the source is 1 g/s, and the units of concentration are $\mu g/m^3$. The wind speed = 0.5 m/s, M-O length= −10 m correspond to simulation 2 of Table 1. In panel c, the plume concentration is normalized with the mean of the plume spatial field.
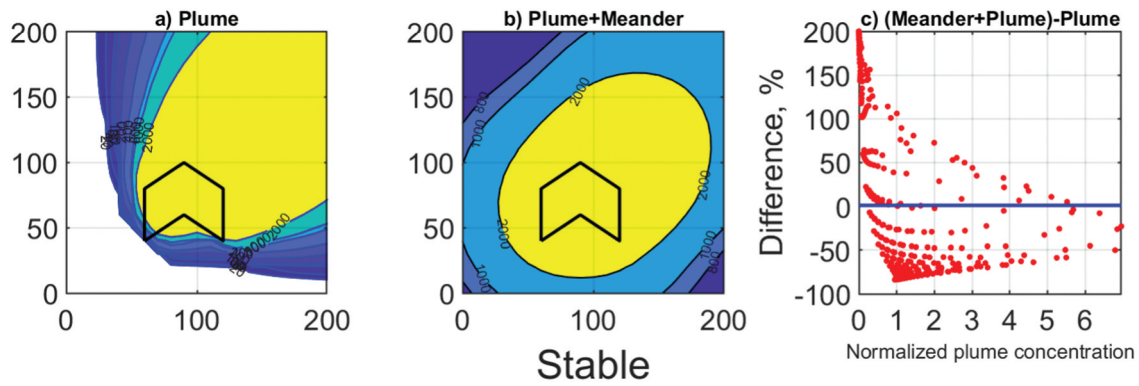
Figure 6. Concentration pattern associated with the polygon area source under stable conditions. The distances shown in the figure are expressed in meters. The emission rate from the source is 1 g/s, and the units of concentration are $\mu g/m^3$. The wind speed = 0.5 m/s, M-O length = 10 m correspond to simulation 3 of Table 1. In panel c, the plume concentration is normalized with the mean of the plume spatial field.
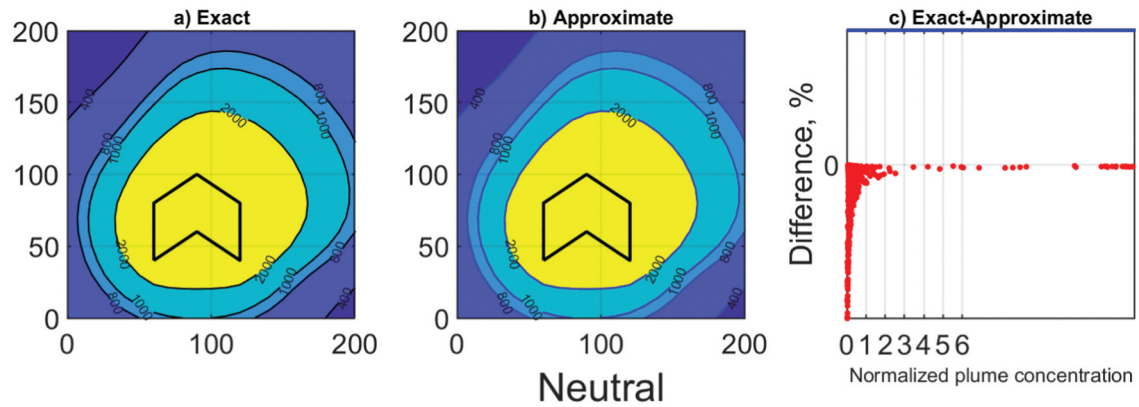

Figure 7. Concentration pattern associated with the polygon area source under neutral conditions and $z_r = z_s = 0$. The distances shown in the figure are expressed in meters. The emission rate from the source is 1 g/s, and the units of concentration are $\mu g/m^3$. The wind speed = 0.5 m/s, M-O length= −1000 m. In panel c, the plume concentration is normalized with the mean of the exact spatial field.

Figure 8. Concentration pattern associated with the polygon area source under neutral conditions and $z_r = z_s = 1$ m. The distances shown in the figure are expressed in meters. The emission rate from the source is 1 g/s, and the units of concentration are $\mu g/m^3$. The wind speed= 0.5 m/s, M-O length= −1000 m. In panel c, the plume concentration is normalized with the mean of the exact spatial field.
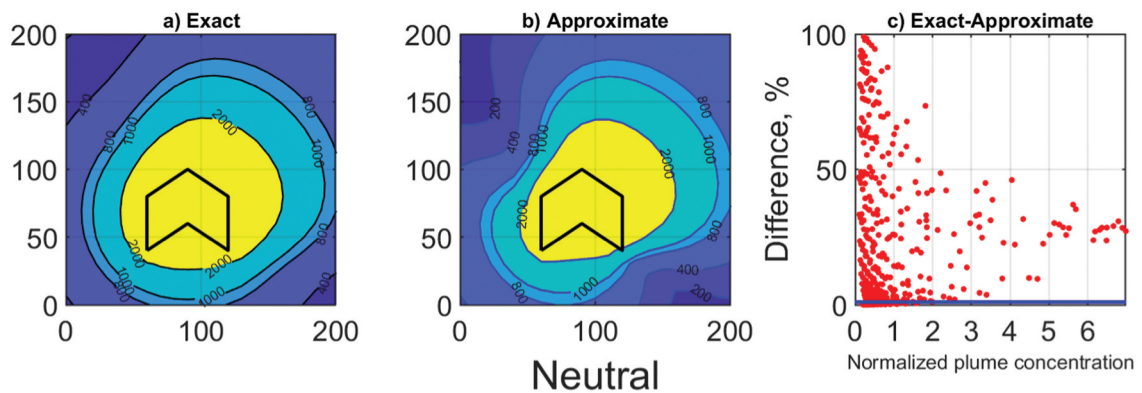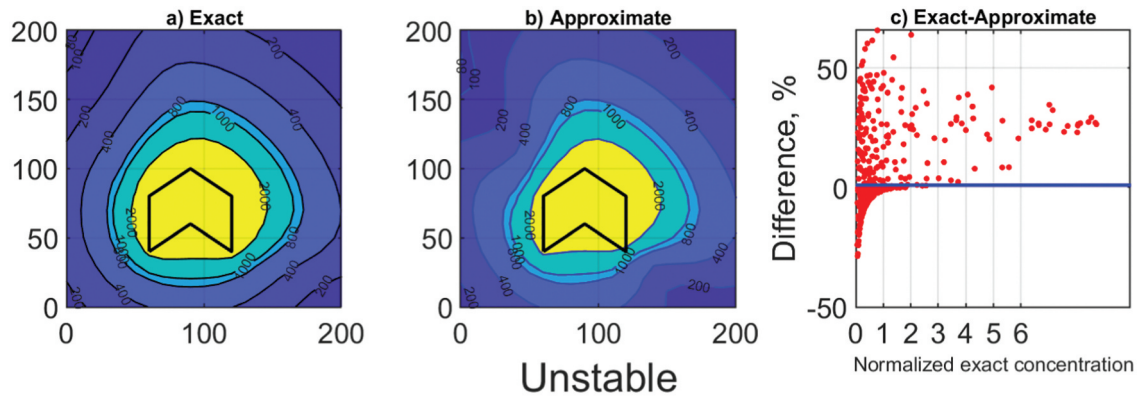
Figure 9. Concentration pattern associated with the polygon area source under unstable conditions and $z_r = z_s = 1$ m. The distances shown in the figure are expressed in meters. The emission rate from the source is 1 g/s, and the units of concentration are $\mu g/m^3$. The wind speed= 0.5 m/s, M-O length= -10 m. In panel c, the plume concentration is normalized with the mean of the exact spatial field.

Figure 10. Concentration pattern associated with the polygon area source under stable conditions and $z_r = z_s = 1$ m. The distances shown in the figure are expressed in meters. The emission rate from the source is 1 g/s, and the units of concentration are $\mu g/m^3$. The wind speed= 0.5 m/s, M-O length= 10 m. In panel c, the plume concentration is normalized with the mean of the exact spatial field.
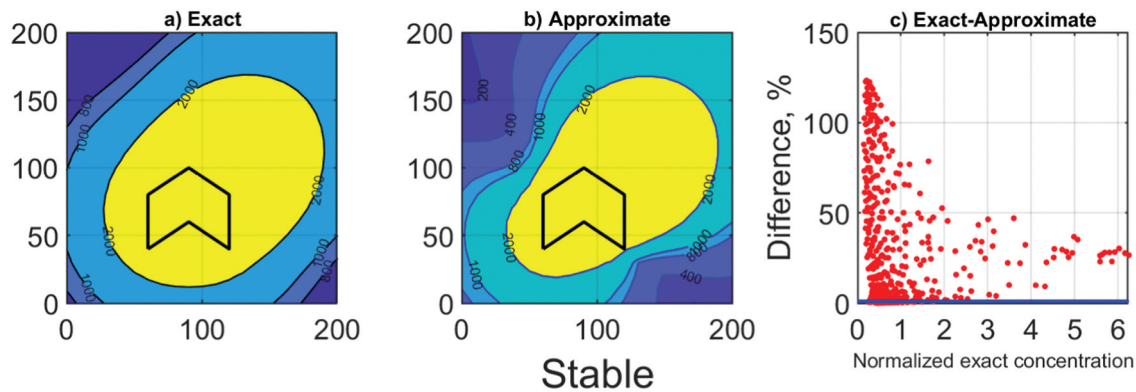
Table 2. Meteorological inputs and differences associated with approximating meander in the area source algorithm. f_r is the meander weighting factor defined in equation 3.

Simulation Number	Scalar Wind Speed(m/s)	M-O Length(m)	f_r	Exact Mean $\mu g/m^3$	Fractional Bias %	Standard Deviation of difference/Mean
1	0.5	−1000	0.72	1905	24.0	0.35
2	0.5	−10	0.72	1280	23.2	0.41
3	0.5	10	0.72	3001	23.2	0.31
4	1	−10	0.18	645	11.3	0.24

and receptor heights are not zero, $z_r = z_s = 1$ m. The approximation underestimates concentrations by about 25% as indicated by the fractional bias. Figures 9 and 10 show that the results are similar when the meteorological conditions are unstable or stable. Table 2 indicates that the normalized standard deviation of the errors during unstable conditions is 0.4 which is about 25% higher than during stable conditions for this specific set of simulations. We have conducted several simulations with different sets of release height, receptor height, wind speed, and MO length, and example of which is

shown in Table 2. The results indicate that the fractional bias does not exceed 25%, which suggests that it might be possible to generalize the result that the maximum fractional bias between the exact and approximate representation of meander is 25%.

Discussion and conclusion

We note that this formulation for meandering depends on a weighting factor, f_r, in Equation (3), whose

functional form is arbitrary. We can avoid this problem by using an alternative approach that expresses the concentration in polar co-ordinates. As pointed out by Hanna et al. (2003), and formalized by Venkatram et al. (2004), the concentration associated with a point source can also be expressed in polar co-ordinates

$$C(\theta, z_s, z_r) = Q\frac{P(\theta)}{U_s r}V(z_s, z_r, r) \qquad (12)$$

where θ is the angle between the line joining the source to the receptor and the mean wind direction, and $P(\theta)$ is the distribution of wind directions about the mean wind direction. In a field study conducted in an urban location, Venkatram et al. (2004) found that this wind direction distribution was close to Gaussian until the horizontal turbulent intensity σ_v/U_s exceeds 5,

$$P(\theta) = \frac{1}{\sqrt{2\pi}\sigma_\theta}\exp\left(-\frac{\theta^2}{2\sigma_\theta^2}\right) \qquad (13)$$

where σ_θ is the standard deviation of the wind direction fluctuations about the mean wind direction. Its magnitude determines the impact of the point source at upwind locations. So, this formulation automatically accounts for meandering and thus avoids the arbitrariness of the formulation of the weighting factor, f_r, in Equation (3). A semi-empirical equation (Venkatram et al. 2004) that relates σ_θ to σ_v is

$$\sigma_\theta = \frac{\pi}{\sqrt{3}}\tanh\left(\frac{\sigma_v}{U_v}\frac{\sqrt{3}}{\pi}\right), \qquad (14)$$

which keeps the value of σ_θ between σ_v/U_v and $\pi/\sqrt{3}$ for large σ_v/U_v when $P(\theta)$ becomes uniform over 2π.

When applied to a line source perpendicular to the wind direction, the concentration can be expressed as in Equation (6)

$$C(x_r, y_r, z_r) = q\int_{y_1}^{y_2}P(\theta)\frac{V(z_s, z_r, r)dy}{U_s r},$$

$$and$$

$$\theta = \tan^{-1}(y_r - y, x_r) \qquad (15)$$

where x_r is the perpendicular distance of the receptor to the line source. Evaluation of Equation (15) requires numerical integration as in the previous case. However, if $z_s = z_r = 0$, and $\sigma_z \sim x$, Equation (15) has the analytical solution

$$C(x_r, y_r, z_r) = \sqrt{\frac{2}{\pi}}\frac{q}{\sigma_z(x_r)U_s}\frac{(erf(t_2) - erf(t_1))}{2}$$

$$t_2 = \frac{\theta_2}{\sqrt{2}\sigma_\theta} \ and \ t_1 = \frac{\theta_1}{\sqrt{2}\sigma_\theta}$$

$$\theta_2 = \tan^{-1}\left(\frac{y_2 - y_r}{x_r}\right) \ and \ \theta_1 = \tan^{-1}\left(\frac{y_1 - y_r}{x_r}\right) \qquad (16)$$

where $erf(t)$ is the error function given by $erf(t) = \sqrt{\frac{2}{\pi}}\int_0^t e^{-x^2}dx$. When $x_r < 0$, the receptor is upwind of the line source, which requires the integral to be expressed as the sum of two integrals, one between θ_2 and π, and the other between θ_1 and $-\pi$.

The scope of this paper does not allow a comparison between these two approaches to treating meander. However, it is useful to show that these approaches yield significantly different concentration patterns as illustrated in Figure 11. The "pancake" approach spreads the concentration pattern further upwind than the "theta" approach, but decreases the concentrations downwind of the source relative the "theta" approach. This results in a fractional bias between these two
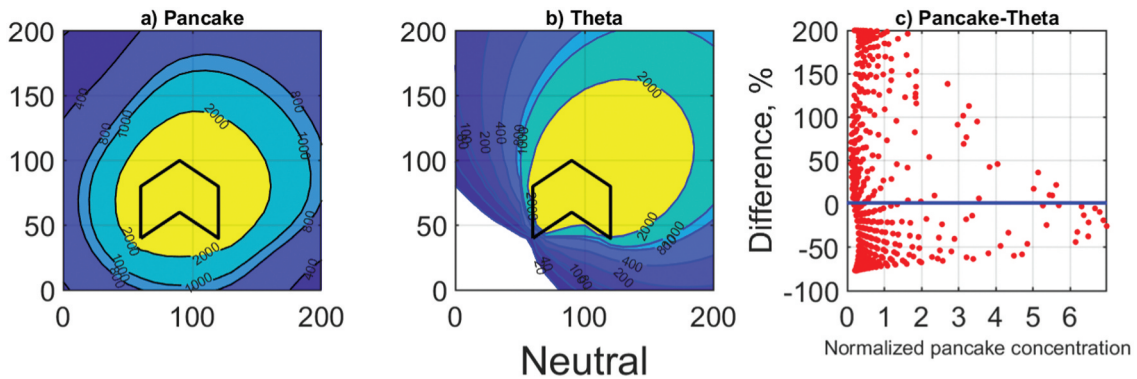

Figure 11. Comparison of concentration patterns produced by two different formulations of meander: pancake refers to equations 3 and theta refers to equation (12). The simulation corresponds to neutral conditions with M-O length=−1000 m, wind speed= 0.5 m/s and $z_r = z_s = 1$ m. The distances shown in the figure are expressed in meters. The emission rate from the source is 1 g/s, and the units of concentration are $\mu g/m^3$. In panel c, the plume concentration is normalized with the mean of the pancake spatial field.

patterns of −22% indicating the higher downwind concentrations of the "theta" approach.

As expected, the introduction of meandering decreases concentrations downwind of the area source and creates concentrations upwind of the source. The two approaches to meandering yield significantly different results when meandering is a factor. The U.S. National Oceanic and Atmospheric Administration (NOAA) conducted a tracer field study in 1974 at Idaho Falls (Sagendorf and Dickson 1974) to make measurements of dispersion from a point source under stable conditions when the wind speeds were less than 2 m/s at 4 m on a 61 m tower; the winds were measured at 6 levels on this tower with cup anemometers and bivanes. The temperature was also measured at these levels. The tracer, sulfur hexafluoride, released at 1.5 m, was sampled with bag samplers laid out in radii at 100, 200, and 400 m at 6^0 intervals. The data from the 14 experiments conducted during this study have been examined by several investigators (Cirillo and Poli 1992; Sharan and Yadav 1998) using different approaches to account for meandering under low wind speeds, which included diffusion along the wind. Analysis of this data by Qian and Venkatram (2011) suggests that the "pancake" approach, Equations (1)–(3), improves model estimates for point sources during low winds. This result is tentative because turbulence parameters, which govern dispersion, were inferred, not measured using instrumentation such as sonic anemometers. In summary, the data from the NOAA study do not allow one to choose one approach over another in modeling dispersion under low winds.

Data from a more recent field study conducted in Riverside, California (Venkatram et al. 2004), suggest that the "theta" approach, Equations (12) and (13), yields acceptable results for line sources until the horizontal turbulent intensity, σ_v/U_s, exceeds 5. This formulation avoids the arbitrariness of the choice of the weighting factor in Equation (3). However, incorporating it in AERMOD cannot be readily justified because all the receptors in the field study were located within 20 m from the source. In view of the importance of area sources, there is a need for a comprehensive field study with modern instrumentation to evaluate the models that treat area sources, especially under low wind speeds.

The inclusion of meandering increases the computational demands of the already resource-hungry algorithm for estimating the impact of area sources when the wind speeds are comparable to the standard deviation of the horizontal velocity fluctuations. We have proposed an approximation that reduces the computational demand by over a factor of 30. However, it underestimates concentrations relative to those from the numerical integration required to implement meandering. A limited number of simulations indicates that the fractional bias does not exceed 25%. This suggests that it might be possible to adopt the analytical approximation for meandering by multiplying the results it produces by an appropriate factor, say 1.3.

Acknowledgment

Disclosure statement

No potential conflict of interest was reported by the author(s).

Funding

About the authors

Akula Venkatram is a Professor of Mechanical Engineering at the University of California at Riverside.

Gavendra Pandey is a Research Associate at the Institute for the Environment, University of North Carolina at Chapel Hill, NC, USA.

Saravanan Arunachalam is a Research Professor and Deputy Director of the Institute for the Environment, University of North Carolina at Chapel Hill, NC, USA.

Data availability statement

The data used in this study can be requested from the corresponding author, Akula Venkatram.

References

Anfossi, D., S. Alessandrini, S. Trini Castelli, E. Ferrero, D. Oettl, and G. Degrazia. 2006. Tracer dispersion simulation in low wind speed conditions with a new 2D Langevin equation system. *Atmos. Environ.* 40 (37):7234–45. doi:10.1016/j.atmosenv.2006.05.081.

Brusasca, G., G. Tinarelli, and D. Anfossi. 1992. Particle model simulation of diffusion in low wind speed stable conditions. *Atmos. Environ. Part A Gener. Top.* 26 (4):707–23. doi:10.1016/0960-1686(92)90182-K.

Carruthers, D.J., R.J. Holroyd, J.C.R. Hunt, W.S. Weng, A. G. Robins, D.D. Apsley, D.J. Thompson, and F.B. Smith.

1994. UK-ADMS: A new approach to modelling dispersion in the earth's atmospheric boundary layer. *J. Wind Eng. Ind. Aerodyn.* 52 (C):139–53. doi:10.1016/0167-6105(94)90044-2.

Cimorelli, A.J., S.G. Perry, A. Venkatram, J.C. Weil, R.J. Paine, R.B. Wilson, R.F. Lee, W.D. Peters, and R.W. Brode. 2005. AERMOD: A dispersion model for industrial source applications. Part I: General model formulation and boundary layer characterization. *J. Appl. Meteorol.* 44 (5):682–93. doi:10.1175/JAM2227.1.

Cirillo, M.C., and A.A. Poli. 1992. An intercomparison of semiempirical diffusion models under low wind speed, stable conditions. *Atmos. Environ. Part A Gener. Top.* 26 (5):765–74. doi:10.1016/0960-1686(92)90236-E.

Hanna, S.R., R. Britter, P. Franzese, and E. Baja. 2003. A simple urban dispersion model tested with tracer data from Oklahoma City and Manhattan. *Atmos. Environ.* 37 (36):778–86. doi: 10.1016/j.atmosenv.2003.08.014.

Hanna, S.R., and B. Chowdhury. 2014. Minimum turbulence assumptions and u* and L estimation for dispersion models during low-wind stable conditions. *J. Air Waste Manag. Assoc.* 64 (3):309–21. doi: 10.1080/10962247.2013.872709.

Oettl, D., R.A. Almbauer, and P.J. Sturm. 2001. A new method to estimate diffusion in stable, low-wind conditions. *J. Appl. Meteorol.* 40 (2):259–68. doi: 10.1175/1520-0450(2001).

Press, W.H., S.A. Teukolsky, W.T. Vetterling, and B.P. Flannery. 1996. *Numerical recipes: The art of scientific computing.* New York, NY, USA: Cambridge University Press.

Qian, W., and A. Venkatram. 2011. Performance of steady-state dispersion models under low wind-speed conditions. *Boundary-Layer Meteorol.* 138 (3):475–91. doi:10.1007/s10546-010-9565-1.

Sagendorf, J.F., and C.R. Dickson. 1974. *Diffusion under low windspeed, inversion conditions.* IDAHO Falls, IDAHO, USA: U.S. National Oceanic and Atmospheric Administration Technical Memorandum ERL ARL-52.

Sharan, M., and A.K. Yadav. 1998. Simulation of diffusion experiments under light wind, stable conditions by a variable K-theory model. *Atmos. Environ.* 32 (20):3481–92. doi:10.1016/S1352-2310(98)00048-X.

Venkatram, A., V. Isakov, J. Yuan, and D. Pankratz. 2004. Modeling dispersion at distances of meters from urban sources. *Atmos. Environ.* 38 (28):4633–41. doi:10.1016/j.atmosenv.2004.05.018.

Venkatram, A., and R.R. Thiruvenkatachari. 2023. Accounting for area sources in air pollution models. *Int. J. Environ. Res. Public Health* 20 (12):6110. doi: 10.3390/ijerph20126110.

Technical Report Documentation Page

1. Report No.	2. Government Accession No.	3. Recipient's Catalog No.
4. Title and Subtitle		5. Report Date
		6. Performing Organization Code
7. Author(s)		8. Performing Organization Report No.
9. Performing Organization Name and Address		10. Work Unit No. (TRAIS)
		11. Contract or Grant No.
12. Sponsoring Agency Name and Address		13. Type of Report and Period Covered
		14. Sponsoring Agency Code
15. Supplementary Notes		
16. Abstract		
17. Key Words	18. Distribution Statement	

19. Security Classif. (of this report)	20. Security Classif. (of this page)	21. No. of Pages	22. Price
Unclassified	Unclassified		

Form DOT F 1700.7 (8-72)   Reproduction of completed page authorized